Latency-dependent filtering and compact representation of the complete auditory pathway response

Angel de la Torre,[1] Joaquin T. Valderrama,[2, a)] Jose C. Segura,[1] and Isaac M. Alvarez[1]

[1]*Department of Signal Theory, Telematics, and Communications, University of Granada, Granada, Spain*

[2]*National Acoustic Laboratories, Sydney, Australia*

(Dated: 7 July 2020)

Auditory evoked potentials (AEPs) include the auditory brainstem response (ABR), middle latency response (MLR) and cortical auditory evoked potentials (CAEPs), each one covering a specific latency range and frequency band. For this reason, ABR, MLR and CAEP are usually recorded separately using different protocols. This article proposes a procedure providing a latency-dependent filtering and down-sampling of the AEP responses. This way, each AEP component is appropriately filtered, according to its latency, and the complete auditory pathway response is conveniently represented (with the minimum number of samples, i.e., without unnecessary redundancies). The compact representation of the complete response facilitates a comprehensive analysis of the evoked potentials (keeping the natural continuity related to the neural activity transmission along the auditory pathway), which provides a new perspective in the design and analysis of AEP experiments. Additionally, the proposed compact representation reduces the storage or transmission requirements when large databases are manipulated for clinical or research purposes. The analysis of the AEP responses shows that a compact representation with 40 samples/decade (around 120 samples) is enough for accurately representing the response of the complete auditory pathway and provides appropriate latency-dependent filtering. MatLab/Octave code implementing the proposed procedure is included in the supplementary materials.

Keywords: Auditory Evoked Potentials (AEPs); auditory pathway; electroencephalogram (EEG); auditory brainstem response (ABR); middle latency response (MLR); cortical auditory evoked potentials (CAEPs).

[a)]Also at: Department of Linguistics, Macquarie University, Sydney, Australia. Electronic mail: joaquin.valderrama@nal.gov.au

I. INTRODUCTION

Auditory evoked potentials (AEPs) are registered by presenting an auditory stimulus and recording the neural activity elicited by the stimulus. Due to the noise affecting the recording procedure and the low amplitude of the responses (typically in the range of microvolts), a number of responses are synchronously averaged in order to improve the signal to noise ratio (SNR) (Thornton, 2007).

Conventional recording procedures configure a minimal separation between consecutive stimuli greater than the response duration in order to avoid interference among adjacent responses (Woldorff, 1993). This requirement has conditioned the protocols for recording AEP responses, with different configurations for each portion of the response. For instance, the auditory brainstem response (ABR) includes waves I, II, III, IV, V and VII, with latencies in the range 1-10 ms. Conventional ABR recording protocols configure an inter-stimulus interval (ISI) greater than 15 ms, and a band-pass filtering of the electroencephalogram (EEG) in the band 100-3 000 Hz, removing the later responses (in the frequency band below 100 Hz) as well as the high frequency noise (above 3 kHz) (Burkard and Don, 2007). Similarly, the middle latency response (MLR) includes waves N_0, P_0, N_a, P_a, N_b and P_b in the latency range 10-100 ms. Therefore, recording windows of 100 ms, ISI greater than 120 ms and EEG band-pass filtering in the band 10-300 Hz are considered in the conventional MLR recording protocol (Pratt, 2007). Finally, the cortical auditory evoked potentials (CAEP), with waves P_1, N_1, P_2, N_2 and P_3 between 50 and 500 ms, are conventionally recorded with protocols using recording windows of 1 s, ISI greater than this window and EEG band-pass

filtering in the band 1-30 Hz (removing high frequency noise as well as earlier responses) (Martin *et al.*, 2007). The bandwidth limit (due to the band-pass filtering) allows EEG acquisition at appropriate sampling rates (10 kHz, 1 kHz and 100 Hz for ABR, MLR and CAEP, respectively) without information loss, according to the sampling theorem.

In the last decades, AEPs evoked by stimuli presented at high rate have offered new perspectives in audiology. The possibility of recovering the evoked response when the interval between stimuli is shorter than the response duration allows the study of different adaptation mechanisms (Gillespie and Muller, 2009; Thornton and Coleman, 1975) as well as the analysis of the AEP response to progressively more natural stimuli (Maddox and Lee, 2018). Some procedures have been proposed for recording evoked potentials at high stimulation rates: maximum length sequences (MLS) (Eysholdt and Schreiner, 1982; Thornton and Slaven, 1993), adjacent-responses (ADJAR) (Woldorff, 1993), quasi-periodic sequence deconvolution (QSD) (Jewett *et al.*, 2004), continuous loop averaging deconvolution (CLAD) (Bohorquez and Ozdamar, 2006; Ozdamar and Bohorquez, 2006), linear deconvolution for baseline correction (LDBC) (Lütkenhöner, 2010), randomized stimulation and averaging (RSA) (Valderrama *et al.*, 2012), iterative randomized stimulation and averaging (IRSA) (de la Torre *et al.*, 2019; Valderrama *et al.*, 2014b, 2016) and least-squares deconvolution (LS) (Bardy *et al.*, 2014a,b).

The overcoming of the ISI restriction allows the simultaneous recording of the different portions of the AEP response (ABR, MLR and CAEP) at moderate or high stimulation rate (de la Torre *et al.*, 2019; Holt and Ozdamar, 2016; Kohl *et al.*, 2019). The analysis of such response provides information about the whole auditory pathway taking into consideration

all the involved waves, instead of a separated analysis of the different groups of waves in different representations. The simultaneous analysis of all the waves (and their changes associated to the modification of the stimulation parameters) provides new perspectives in the study of the auditory system and its response to stimulation patterns progressively more complex, from those so simple as quasi-periodic sequences of clicks to those so complex as natural speech. Additionally, the analysis of the complete auditory pathway response eliminates the discontinuity usually established among the different groups of waves. This discontinuity does not exists in the generation of the neural activity and is a consequence of the conventional protocols for the acquisition of the evoked responses.

The acquisition of evoked responses from the whole auditory pathway (including ABR, MLR and CAEP) presents some difficulties. On one hand, the appropriate filtering is different for each portion. This is usually solved by applying the less restrictive filtering to the EEG (using the band 1-3000 Hz), but the late portion of the response is more affected by noise (compared with conventional recording procedures). On the other hand, the representation of the whole response requires a high sampling rate associated to the bandwidth of the earlier waves (10 kHz) and a long duration of the response associated to the latencies of the later waves (1 000 ms), which implies a large number of samples to represent the response (typically around 10 000 samples) (de la Torre *et al.*, 2019). In order to illustrate the highly redundant representation of the whole response we can compare these 10 000 samples with those required for representing each portion separately: 100 samples for ABR (10 ms at a sampling rate of 10 kHz), 100 samples for MLR (100 ms at 1 kHz) and 100 samples for CAEP (1 000 ms at 100 Hz), i.e. a total of 300 samples.

Of course, the reason behind these differences is the application of specific filtering and sampling rate to each component (ABR, MLR and CAEP) when they are independently represented, according to the expected frequency content (which changes with the latency). This allows an specific filtering of each portion, providing appropriate noise reduction and compact representation (independent for ABR, MLR and CAEP) but generates the discontinuity in the representation of the auditory pathway response.

In general, a band-limited signal can be low-pass filtered (to remove high-frequency noise) and sampled with a sampling rate at least twice the maximum frequency component (to reduce the number of samples required to represent it) without information loss, since the sampling theorem guarantees that the original signal can be recovered from the samples. Similarly, the evoked response of the complete auditory pathway, with a band limit depending on the latency (the later the waves the narrower bandwidth), can be processed to apply a latency-dependent low-pass filtering and down-sampling, in order to improve both the filtering (to reduce the high-frequency noise) and the representation (to reduce the number of samples required for properly representing the response). This article proposes a digital procedure to provide this latency-dependent low-pass filtering and down-sampling for the evoked response of the complete auditory pathway. The procedure is based on a non-uniform sampling (involving a compression of the latency axis) of the signal representing the AEP response. The compression, approximately logarithmic, provides a bandwidth limitation in terms of the maximum number of oscillations per decade, as well as the sampling rate in terms of number of samples per decade (where a decade in the latency axis is the interval between a latency t_0 and a latency $10 \cdot t_0$).

The proposed procedure is described with a matrix formulation, where the evoked response is represented as a signal with J samples (or a J-component column vector), the reduced representation of the evoked response (after the latency-dependent filtering and down-sampling) as a signal with J_r samples (or a J_r-component column vector, with $J_r < J$), and the latency-dependent filtering and down-sampling procedure is represented as a matrix with J_r rows and J columns. The matrix processes the original AEP response and provides its reduced representation, and also allows to recover, from the reduced representation, the filtered AEP response in the original representation (i.e., from the compact representation with J_r samples, it provides the signal in the conventional representation with J samples at the original sampling rate, including the latency-dependent filtering).

The proposed procedure is described in this article and MatLab/Octave code to generate the latency-dependent low-pass filtering and down-sampling matrix is provided in the supplementary materials. The procedure has been evaluated in experiments involving the simultaneous recording of ABR, MLR and CAEP using clicks as stimuli, presented at different stimulation rates.

II. FORMULATION OF THE LATENCY-DEPENDENT LOW-PASS FILTERING AND DOWN-SAMPLING

A. Matrix formulation of filtering and down-sampling

Let's suppose a digital signal $x(j)$ representing an AEP response. Low-pass filtering is obtained as the convolution of the signal $x(j)$ with the impulsive response of the filter, $h_{lp}(j)$,

as:

$$x_{lp}(j) = h_{lp}(j) * x(j) = \sum_{j'} h_{lp}(j') \cdot x(j - j') \tag{1}$$

where '$*$' represents convolution. If the signal $x(j)$ contains J samples ($j = 0, \ldots, J-1$), it can be represented as a J-component column vector, and filtering can be represented as a matrix product:

$$\mathbf{x}_{lp} = H_{lp}\mathbf{x} \tag{2}$$

where $\mathbf{x}_{lp}$ is a J-component column vector representing the filtered signal and H_{lp} is the $J \times J$ convolution matrix with elements $H_{lp}(j_1, j_2) = h_{lp}(j_1 - j_2)$. The matrix product can be interpreted as a linear operator in the J-dimensional vectorial space representing the digital signals: each filtered sample $x_{lp}(j)$ is obtained as a linear combination of the samples of the original signal, according to the j^{th} row of the convolution matrix.

The low-pass filtered signal can be down-sampled without information loss if the new sampling rate is, at least, twice the maximum frequency component (according to the sampling theorem). In order to down-sample the filtered signal with a factor q, from every q samples 1 sample should be preserved and $q - 1$ samples should be discarded:

$$x_r(j_r) = x_{lp}(j_r \cdot q) \tag{3}$$

where $j_r = 0, \ldots, J_r - 1$ (with $J_r = J/q$), and r refers to the reduced representation after down-sampling. The low-pass filtering and down-sampling operation can also be represented in matrix notation:

$$\mathbf{x}_r = H_r\mathbf{x} \tag{4}$$

where H_r is the matrix H_{lp} preserving 1 of every q rows (i.e., a $J_r \times J$ matrix). Again, this matrix product can be considered a linear transformation from the original representation of the signal (with J components) to a reduced representation (with J_r components), where each new component $x_r(j_r)$ is obtained as a linear combination of all the original components $x(j)$ according to the j_r^{th} row of the matrix H_r. The supplementary materials[1] (Section 1) describe in detail the matrix formulation of filtering and down-sampling.

B. Latency-dependent filtering and down-sampling

A latency-dependent filtering implies that each filtered component $x_{lp}(j)$, is obtained using a different impulsive response, depending on its latency. In other words, while in conventional filtering all the rows of the matrix H_{lp} are identical except for the delay (and all the elements in each direct diagonal of the matrix are identical), latency-dependent filtering can be implemented using a different impulsive response for each row of the matrix. This way, each filtered sample at latency j can be obtained with a latency-specific bandwidth (using an appropriate impulsive response) as a linear combination of the original samples around this latency.

Similarly, latency specific down-sampling can be implemented by selecting the new samples with a latency-dependent down-sampling factor q (according to the latency-dependent bandwidth, in order to locally follow the sampling theorem condition and prevent information loss). The latency-dependent down-sampling can also be implemented as a matrix operation, using a reduced matrix H_r in which the rows are non-uniformly selected from

the matrix H_{lp}. Section 2 of the supplementary materials[1] describes in detail the matrix formulation of the latency-dependent filtering and down-sampling.

C. Bandwidth required at each latency

The latency-dependent low-pass filtering and down-sampling has to be designed taking into account the expected frequency content (and therefore the required bandwidth) of the AEP responses at each latency. The different waves of the AEP responses are narrower at earlier latency and wider at later latency, and the required bandwidth decreases as the latency increases. Taking into account the latency range of the waves and the typical cut-off frequencies used for recording ABR, MLR and CAEP responses, the required bandwidth can be determined for each latency. The waves of ABR are observed at latencies between 1 and 10 ms, and recording protocols apply typically a 3 kHz low-pass filtering in order to preserve the waves and reduce the high frequency noise. Similarly, MLR recording procedures, with waves between 10 ms and 100 ms typically apply 300 Hz low-pass filtering. Finally, CAEP are usually recorded with a 30 Hz low-pass filtering to preserve waves in the latencies between 50 ms and 1 s and remove the high frequency noise. Therefore, a latency-dependent filtering preserving a bandwidth of 3 KHz at 1 ms, 300 Hz at 10 ms, and 30 Hz at 50 ms would be enough for an appropriate representation of the AEP responses.

D. Compression of the latency axis

The latency-dependent low-pass filtering and down-sampling can be implemented as a uniform low-pass filtering and down-sampling performed after a compression of the latency

axis. The progressive reduction of the bandwidth with the latency suggests a logarithmic scaling of the latency axis, which would be described as a non-uniform sampling with K_{dec} samples per decade (i.e., a constant number of samples between a given latency t_0 and a latency $10 \cdot t_0$). The response in the original representation contains samples at the time values:

$$t_j = j \; T_s \tag{5}$$

where $T_s = 1/f_s$ is the sampling period and f_s is the sampling rate. The uniform sampling in a logarithmically compressed latency axis, for K_{dec} samples per decade, would be described with the equation:

$$j_r(t) = K_{dec} \log_{10}(t/T_s) \tag{6}$$

where the samples should be taken at those values of t providing an integer value of $j_r(t)$. This latency compression would be appropriate for large latencies (much greater than T_s) (since an increment of t in a factor 10 would produce an increment of K_{dec} samples, providing K_{dec} samples per decade). However, it is not appropriate at small latency, because the sampling rate would be very large when t is small compared with T_s. Instead, a linear-logarithmic (lin-log) compression can be applied to the latency axis, providing a linear sampling at small latency (compared with the original sampling period) and a logarithmic sampling at large latency. The equation providing the relation between the original time axis and the compressed samples, with a linear compression at small latency (with a maximum sampling rate equal to f_s) and K_{dec} samples per decade at large latency, is:

$$j_r(t) = K_{dec} \log_{10} \left(\frac{t}{T_s} \; \frac{\ln(10)}{K_{dec}} + 1 \right) \tag{7}$$

	K_{dec} = 40 samp/dec		K_{dec} = 60 samp/dec	
latency	f_s=14.7 kHz	f_s=25 kHz	f_s=14.7 kHz	f_s=25 kHz
1 ms	7.96 kHz	10.25 kHz	9.40 kHz	12.76 kHz
2 ms	5.46 kHz	6.45 kHz	6.91 kHz	8.57 kHz
5 ms	2.81 kHz	3.05 kHz	3.85 kHz	4.31 kHz
10 ms	1.55 kHz	1.62 kHz	2.21 kHz	2.36 kHz
20 ms	820.1 Hz	839.4 Hz	1.20 kHz	1.24 kHz
50 ms	339.4 Hz	342.7 Hz	503.3 Hz	510.5 Hz
100 ms	171.7 Hz	172.5 Hz	256.0 Hz	257.9 Hz
200 ms	86.3 Hz	86.6 Hz	129.1 Hz	129.6 Hz
500 ms	34.7 Hz	34.7 Hz	51.9 Hz	52.0 Hz
1000 ms	17.4 Hz	17.4 Hz	26.0 Hz	26.0 Hz

TABLE I. Latency-dependent sampling rate $f'_s(t)$ for different original sampling rates (f_s) and resolutions (K_{dec}) in the compressed latency axis.

where ln() is the natural logarithm (the mathematical derivation of this equation is included in the supplementary materials[1], Section 3). The sampling period can be estimated from this equation as the derivative $\partial t(j_r)/\partial j_r$, or equivalently as the inverse of the derivative $\partial j_r(t)/\partial t$. The latency-dependent sampling period and sampling rate are, respectively:

$$T'_s(t) = \left.\frac{\partial t(j_r)}{\partial j_r}\right|_t = T_s + t\frac{\ln(10)}{K_{dec}} \qquad f'_s(t) = \frac{1}{T'_s(t)} \tag{8}$$

As can be observed from this equation, for small latency ($t \ll T_s$), the sampling period is minimum and equal to T_s (the sampling rate takes the maximum value, f_s) and for large latency ($t \gg T_s$), the sampling rate is $f'_s(t) \approx K_{dec}/(t \cdot \ln(10))$, and therefore it decreases as the latency increases, and depends on the latency but not on the original sampling rate.

The bandwidth preserved at each latency depends on the local sampling rate and the frequency response of the latency-dependent low-pass filter. Even though the sampling

theorem limits the bandwidth to half of the sampling rate, i.e., $f'_s(t)/2$, a slightly smaller bandwidth is recommended in order to allow a reasonable implementation of the filters (otherwise the duration of the impulsive response would be too long). Table I shows the local sampling rate $f'_s(t)$ for original sampling rates of 14.7 and 25 kHz, and for resolutions of 40 and 60 samples/decade. All these configurations provide enough bandwidth for the representation of the AEP responses.

E. Design of the low-pass filters

For the latency-dependent low-pass filtering, a root raised-cosine (RRC) filter in the compressed latency axis has been designed (Proakis and Salehi, 2008). Filters in the RRC family (commonly used in digital communications) are low pass filters specified by two parameters: the symbol period T_0 and the roll-off factor α. They provide a constant frequency response up to $(1-\alpha)/(2T_0)$, a monotonic decay up to $(1+\alpha)/(2T_0)$ and a null response for frequencies above this value. Although its theoretical impulsive response is infinite, a truncated version of an RRC filter can be implemented as a linear phase FIR (Finite Impulsive Response) using a time span including a sufficient number of symbol periods. Additionally, RRC responses are orthogonal when they are delayed an integer number of symbol periods. Detailed information about RRC filters is provided in the supplementary materials[1] (Section 4). In this work, RRC filters with a roll-off α=0.2 are used with an impulsive response length of $\pm$14 symbol periods, containing the 99.9980% of the total energy of the theoretical impulsive response. Its frequency response is constant in the range $[0, 0.4/T_0]$, monotonically decreasing in the range $[0.4/T_0, 0.6/T_0]$ and null for frequency greater than

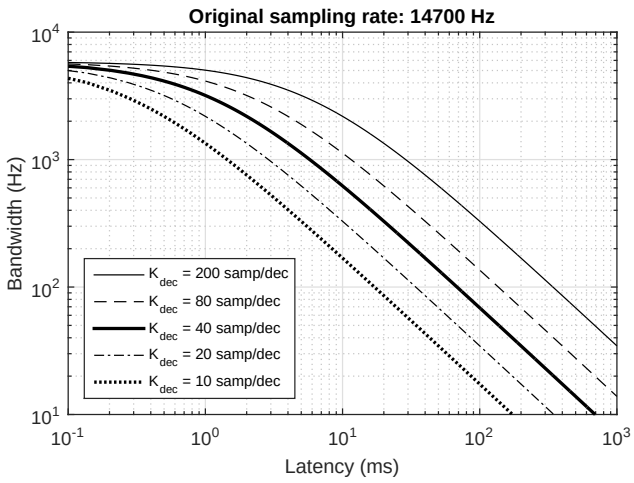

FIG. 1. Bandwidth preserved by the latency dependent filtering using RRC filters with $\alpha = 0.2$.

$0.6/T_0$. A non-causal zero-phase implementation of the filters has been considered in order to avoid delay of the filtered AEP waves.

In order to achieve the latency-dependent low-pass filtering, the time axis of the impulsive response is scaled according to equation (7) (the impulsive response is invariant in the compressed latency axis given by j_r). This latency-dependent low-pass filtering can be represented as a matrix operation H_{lp} where the impulsive response for each latency (represented by each row) is wider as the latency increases (i.e., as we move from top to bottom in the matrix rows). Similarly, the latency-dependent down-sampling can be represented as a reduced matrix H_r, obtained from H_{lp} where only those rows corresponding to the latencies $t(j_r)$ (with j_r integer) are selected.

The RRC filters are designed with a symbol period T_0 matching the sampling period $T_s'(t)$, constant in the compressed latency axis and therefore increasing with the latency according to equation (8). This preserves (without distortion) the frequency range $[0, 0.4] \cdot f_s'$, removes all the frequency components above $0.6 \cdot f_s'$, and produces interference (by aliasing) with the

frequency components in the range $[0.4, 0.6] \cdot f'_s$. If the signal of interest contains, at latency t, only frequency components below $0.4 \cdot f'_s(t)$, the signal is preserved without distortion, and the aliasing only affects the noise components in the range $[0.4, 0.6] \cdot f'_s$. Figure 1 represents the bandwidth preserved by the latency dependent filtering using the proposed RRC filters, for different resolutions (K_{dec} between 10 and 200 samples/decade) and original sampling rate f_s=14 700 Hz. For instance, for K_{dec}=40 samples/decade, the preserved bandwidth is 3 185, 621, 68.6 and 6.94 Hz at latencies 1, 10, 100 and 1000 ms, respectively. Detailed description of the latency-dependent low-pass filtering and down-sampling using RRC filters is provided in the Section 5 of the supplementary materials[1].

F. Orthonormalization of the latency-dependent filtering and down-sampling matrix

The use of a symbol period T_0 equal to the sampling period $T'_s(t)$ in the definition of the RRC filters provides orthogonality between the impulsive responses associated to each sample in the compressed latency axis. However, due to the non-linear compression of the latency axis, the impulsive responses are quasi-orthogonal but not orthogonal in the not-compressed latency axis. Orthonormalization (i.e., orthogonalization and normalization) of the matrix H_r providing the latency-dependent low-pass filtering and down-sampling is highly recommendable because, this way, the matrix provides an equivalent representation of the signals in the subspace of the band-limited signals that preserves the metric in the reduced representation subspace (i.e. the energies or the distances between signals in the original and the reduced representation space are invariant). The representation obtained with an orthonormal matrix is equivalent to the original representation, and therefore all the

estimations or algorithms can be equivalently performed either in the original J-dimensional representation space or in the J_r-dimensional reduced representation space (if the matrix was not orthonormal, the metric in the reduced representation space would be distorted and the results could not be equivalently obtained in the original and the reduced representations).

In order to orthonormalize the matrix H_r, a Gram-Schmidt process is applied. Since the number of remaining rows in the filtering and down-sampling matrix is significantly smaller than the number of columns, an orthonormalization based on Gaussian elimination is proposed. After the orthonormalization, the rows of the matrix V_r constitute an orthonormal basis of functions describing the subspace of the latency-dependent band-limited signals. If V_r is the matrix resulting from the orthonormalization of the H_r matrix, then the product $V_r V_r^T$ (where V_r^T is the transposed of V_r) is the $J_r \times J_r$ identity matrix. The orthonormal matrix V_r can be used to project the original signal to the subspace of the latency-dependent band-limited signals:

$$\mathbf{x}_r = V_r \mathbf{x} \tag{9}$$

This matrix operation removes all the components out of the subspace defined by the basis of functions and provides a compact representation of those components within the subspace of the latency-dependent band limited signals. A MatLab/Octave function providing the orthonormalized latency-dependent low-pass filtering and down-sampling matrix V_r has been implemented (included in the supplementary materials[1], Section 6). This function includes the compression of the latency axis according to equation (7), the definition of J_r responses uniformly distributed in the compressed latency axis and the orthonormalization of the

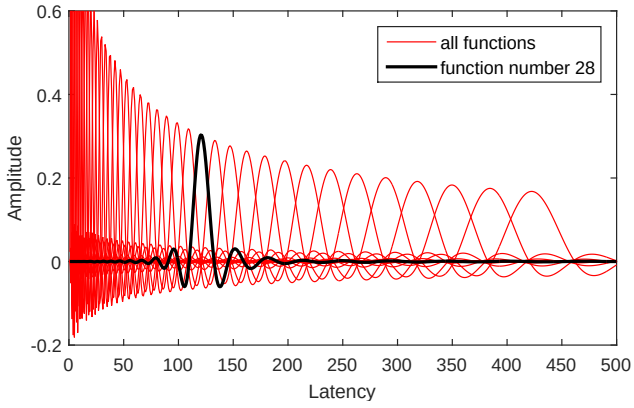

FIG. 2. (Color online) Functions of the orthonormalized basis for J=500 samples and K_{dec}=25 samples/decade.

resulting functions in order to provide the matrix V_r containing the orthonormal basis of the reduced representation space.

Figure 2 represents the functions of the orthonormalized basis (i.e., the rows of the matrix V_r) for the latency-dependent low-pass filtering and down-sampling procedure designed for J=500 samples and K_{dec}=25 samples/decade (resulting in J_r=41). The RRC shape (in the compressed latency axis) can be appreciated in the function represented with the thicker line (corresponding to the 28-th function). Section 7 of the supplementary materials[1] includes some examples of the sampling functions in the matrices H_r and V_r (i.e., before and after the orthonormalization).

G. Reconstruction of the signal in the original representation

Since the matrix V_r is orthonormal, it can be directly applied to transform the reduced representation to the original representation:

$$\mathbf{x}_{lp} = V_r^T \cdot \mathbf{x}_r = V_r^T \cdot V_r \cdot \mathbf{x} \tag{10}$$

This matrix operation provides the latency-dependent filtered signal in the original representation (i.e., at the original sampling rate). Section 8 of the supplementary materials[1] includes some examples comparing the $\mathbf{x}_{lp}$ signal recovered from the previous equation and that obtained by filtering with H_{lp}. Slight differences associated to aliasing are also discussed.

The representation of the latency-dependent low-pass filtered response at the original sampling rate is highly redundant, because at late latency the bandwidth of the response is very small compared with the sampling rate. Instead, the response can be reconstructed at specific latencies. In order to estimate the filtered signal at a specific latency t_i, the contribution of each component in the reduced representation must be considered:

$$x_{lp}(t_i) = \sum_{j_r=0}^{J_r-1} x_r(j_r) V_r(j_r, j(t_i)) \tag{11}$$

where $x_r(j_r)$ is the j_r-th component of the reduced representation $\mathbf{x}_r$ and $V_r(j_r, j(t_i))$ is the j_r-th function of the basis (given by the j_r-th row of the matrix V_r) evaluated (or interpolated) at the latency t_i. This way, from the reduced representation, the filtered response $x_{lp}(t)$ can be evaluated at a reasonable set of latencies $\{t_i\}$ (for example, with 200 samples per decade in the interval between 1 ms to 1 s) providing a representation more natural than the reduced representation $\mathbf{x}_r$ (which modifies the amplitudes depending on the latency due to the orthonormalization of the matrix) and more compact than the representation at the original sampling rate.

The reconstruction of the response at specific latencies has been implemented as a matrix operation. A MatLab/Octave function providing the reconstruction matrix for specific

latencies is included in the supplementary materials[1] (Section 9). Some examples are also included.

III. EXPERIMENTAL RESULTS

The proposed latency-dependent filtering and down-sampling has two objectives: on one hand, to provide a filtering adapted to the AEP spectral content (which changes with the latency) in order to appropriately reduce the high frequency noise; on the other hand, to provide a compact representation of the AEP responses, with a sampling rate adapted to the spectral content (and therefore also changing with the latency), in order to reduce the number of samples required for representing the responses.

The evaluation of the proposed procedure has been performed using both simulations and real AEP responses. Simulations are based on synthetic EEGs, generated with an AEP response used as reference and contaminated with noise. Therefore, since the reference response is available, the noise affecting the estimated responses (either the not-filtered or the latency-dependent filtered) can accurately be evaluated in terms of the SNR. An evaluation of the noise reduction provided by the latency-dependent filtering is more difficult in experiments with recorded EEGs (since the reference response is not available) but provides more realistic results.

A. Experimental design

For the experiments involving simulations, an AEP response has been prepared as reference. This response corresponds to the grand average (estimated from 4 subjects) of an

AEP response to 0.1 ms rarefaction clicks presented at 74 dB (hearing level) at an average rate of 1.39 Hz, with a random inter-stimulus interval (ISI) with uniform distribution in the range 480-960 ms. The acquisition procedure and the response is described in detail in (de la Torre *et al.*, 2019). In spite of the grand average process this response contains some noise (particularly at late latency) due to the noise contaminating the EEGs. For this reason, the AEP response was latency-dependent filtered with a resolution of 40 samples/decade, using the corresponding orthonormalized matrix V_r:

$$\mathbf{x}_{ref} = V_r^T \cdot (V_r \cdot \mathbf{x}_0) \tag{12}$$

where $\mathbf{x}_0$ is the original grand-average AEP response and $\mathbf{x}_{ref}$ is the filtered response used as reference. This resolution has been selected taking into account the spectral content of the AEP responses expected at each latency. The AEP response $\mathbf{x}_{ref}$ (with 14 700 samples at a sampling rate 14.7 kHz, i.e., corresponding to a response length of 1 s.), is described in detail in the supplementary materials[1] (Section 10).

The reference response $\mathbf{x}_{ref}$ was used to generate a synthetic EEG using a random ISI with uniform distribution in the interval 480-960 ms. The EEG was contaminated with pink noise (i.e., with power spectral density decreasing with 3 dB/octave), with a level providing a AEP response with a SNR around 10 dB (which is a typical noise level in AEP experiments). The AEP response $\mathbf{x}$ was estimated from the synthetic EEG using the IRSA algorithm (de la Torre *et al.*, 2019; Valderrama *et al.*, 2014b, 2016). The latency-dependent low-pass filtering was applied to the response with resolutions between 10 and 200 samples/decade ($\mathbf{x}_{lp} = V_r^T \cdot V_r \cdot \mathbf{x}$). The SNR was evaluated as the ratio between the energy of the reference response $\mathbf{x}_{ref}$ and the energy of the noise $\mathbf{n}$ contaminating the

evaluated response, i.e., $\mathbf{n} = \mathbf{x} - \mathbf{x}_{ref}$ for the non filtered response, $\mathbf{n} = \mathbf{x}_{lp} - \mathbf{x}_{ref}$ for the filtered responses. The required number of samples in the reduced representation $\mathbf{x}_r = V_r \cdot \mathbf{x}$ was also evaluated.

In the experiments based on real EEGs, six stimulation rates ranging between 1.39 Hz (for ISI 480-960 ms) and 44.44 Hz (for ISI 15-30 ms) were considered. For each ISI condition, 3 portions of EEG with 228 s were recorded (which accumulates 684 s). Rarefaction clicks of 0.1 ms presented at 74 dB (hearing level) were used as stimulation. The clicks were delivered diotically through ER-3A insert earphones. These transducers (using a delivery tube to separate the electromagnetic interference from the response) cause a group delay of around 1 ms (Elberling *et al.*, 2012). The response estimation is synchronized with the start of each stimulus in the transducer (which allows to appreciate the stimulation artifact at the beginning of the estimated responses), and therefore, since the group delay was not compensated, a delay of about 1 ms is expected in the waves of the evoked responses. The electrical response was recorded with surface electrodes located at Fz (upper forehead, active), Tp10 (right mastoid, reference) and Fpz (middle forehead, ground) using an instrumentation preamplifier (gain 70 dB; bandwidth 1-3 500 Hz) (Valderrama *et al.*, 2013, 2014a,b). The preamplified EEG was digitized (44 100 Hz sampling rate, 16 bits/sample), low-pass filtered (4 000 Hz cut-off frequency) and down-sampled in a factor 3 (14 700 Hz final sampling rate). Eye-blinking artifacts were eliminated with the iterative template matching and suppression algorithm (ITMS) (Valderrama *et al.*, 2018). Eight subjects (aged 26-58 years) participated in this study. The protocol followed in this study is in accordance with the Code of Ethics of the World Medical Association (Declaration of Helsinki) for exper-

iments involving humans and it was approved by the Research Ethics Committee of the University of Granada, reference 961/CEIH/2019. The EEG recordings used in this study are an extension of the database used in a recent study (de la Torre *et al.*, 2019). More details about the experimental procedure can be found in this reference.

As in the case of synthetic EEGs, the AEP responses were obtained from the real EEGs with the IRSA algorithm (de la Torre *et al.*, 2019; Valderrama *et al.*, 2014b, 2016). The latency-dependent low-pass filtering has been applied with resolutions between 5 and 200 samples/decade. In order to evaluate the quality improvement provided by the latency-dependent filtering we have used the three AEP responses estimated from each EEG portion of 228 s: for each subject and ISI condition, the average from the three responses, filtered with K_{dec}=40 samples/decade, was used as reference and the SNR was estimated for each individual response (using the corresponding reference). The resulting individual SNR estimations have been averaged (across subjects, ISI conditions and repetitions). In addition to this estimation of the SNR (independent for each subject), a grand-average-based SNR was estimated: For each ISI condition, the grand-average across subjects from each of the EEG portions of 228 s were used as individual responses, and the average of them, filtered with K_{dec}=40 samples/decade, was used as reference. The SNR was estimated from each grand-average response using the corresponding reference, and the resulting SNR estimations were averaged across ISI conditions and repetitions. The utility of the SNR estimated with these procedures is limited, but they provide an objective comparison of the effect of the latency dependent filtering under two noise conditions (subject-based responses are more affected by noise than grand-average-based responses).

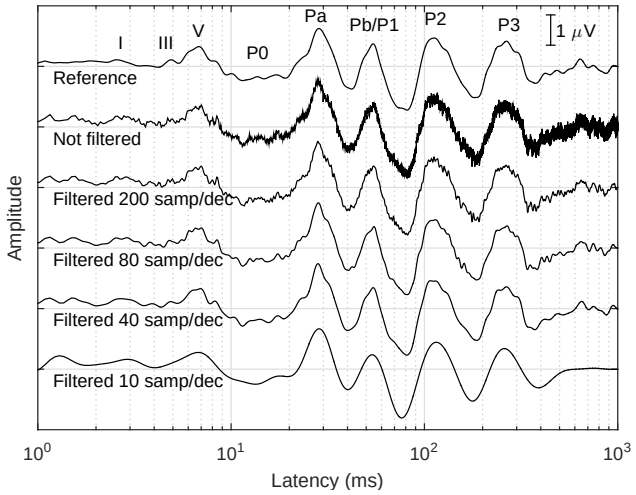

FIG. 3. From top to bottom, the reference AEP response, the IRSA estimation (without filtering) and the latency-dependent filtered responses with 200, 80, 40 and 10 samples/decade. Simulation using a synthetic EEG generated with a real response (for ISI in the range 480-960 ms), contaminated with pink noise.

B. Experimental results with simulations

Figure 3 shows the effect of the latency-dependent low-pass filtering in the experiments involving simulations. The plots represent the AEP responses: reference $\mathbf{x}_{ref}$, not filtered $\mathbf{x}$, and latency-dependent filtered $\mathbf{x}_{lp}$ with resolutions of 200, 80, 40 and 10 samples/decade. Compared with the clean reference response, the not filtered response is affected by noise due to the noise added to the EEG. As observed, the latency-dependent filtering improves the quality of the responses by removing the high frequency noise. The noise reduction is more effective as the latency-dependent filtering is more restrictive. The last plot (for 10 samples/decade) provides the most effective noise reduction, but this filtering is excessive and causes an important distortion in the AEP response. The resolution of 40 samples/decade provides the best balance between noise reduction and distortion. The representation of the

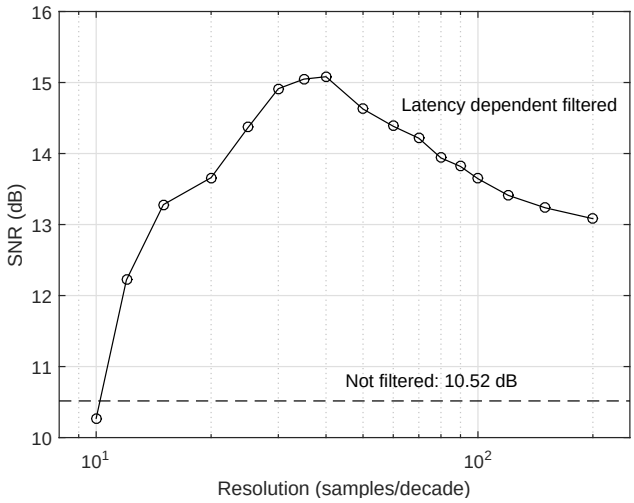

FIG. 4. SNR of the AEP responses as a function of the resolution K_{dec} used in the latency-dependent filtering (solid line with circles). The dashed line represents the SNR for the not filtered response. Results corresponding to simulations; SNR evaluated using $\mathbf{x}_{ref}$ as reference.

not filtered AEP response includes 14 700 samples. In the case of resolutions of 200, 80, 40 and 10 samples/decade, representing the AEP response requires 446, 210, 117 and 35 samples, respectively, which implies a substantial reduction of the dimensionality.

The noise reduction provided by the latency-dependent filtering has been evaluated in terms of the SNR. Figure 4 represents the SNR (using the AEP response $\mathbf{x}_{ref}$ as reference) as a function of the resolution applied in the latency-dependent filtering (solid line with circles). The dashed line is the SNR for the not filtered response (10.52 dB). As observed, the latency-dependent filtering improves the quality by appropriately removing the high frequency noise. The noise reduction is more effective as the filtering is more restrictive, increasing from 13.08 dB (at 200 samples/decade) to around 15 dB (at 40, 35 and 30 samples/decade). As expected, the resolution providing the best results is around 40 samples/decade (which is the resolution used for preparing the reference AEP response). A resolution below 30

samples/decade reduces the SNR due to the distortion caused for so restrictive latency-dependent filtering.

Section 11 of the supplementary materials[1] contains more detailed results involving simulations. Figures similar to 3 and 4 are provided for simulations using white noise and real EEG noise. The behavior with real noise is similar to that with pink noise, with the best performance around 30-40 samples/decade and improvements greater than 4 dB (suggesting pink noise as a reasonable model for EEG contamination). The improvement is more important in the case of white noise (around 20 dB), because high frequency noise is more aggressive in this case (even though this is not a realistic noise model for EEGs). As observed, thanks to the latency-dependent filtering and down-sampling, as the resolution decreases (from 200 to around 40 samples/decade), both the SNR and the dimensionality reduction improve. Beyond 40 samples/decade the latency-dependent filtering is excessive and produces some distortion in the AEP waves.

C. Effect of the latency-dependent filtering with real responses

Taking into account the expected spectral content of the AEP responses, the analysis of table I and the responses estimated in the simulations, a resolution K_{dec}=40 samples/decade has been selected for filtering the AEP responses in the experiments with real recordings. Figure 5 shows the AEP responses for subject 1. The results are represented for different ISI configurations from 480-960 ms (top) to 15-30 ms (bottom). Three plots are shown for each configuration (for consistency evaluation), each one corresponding to the estimation from an EEG portion of 228 s. The plots in the left panel correspond to the not filtered

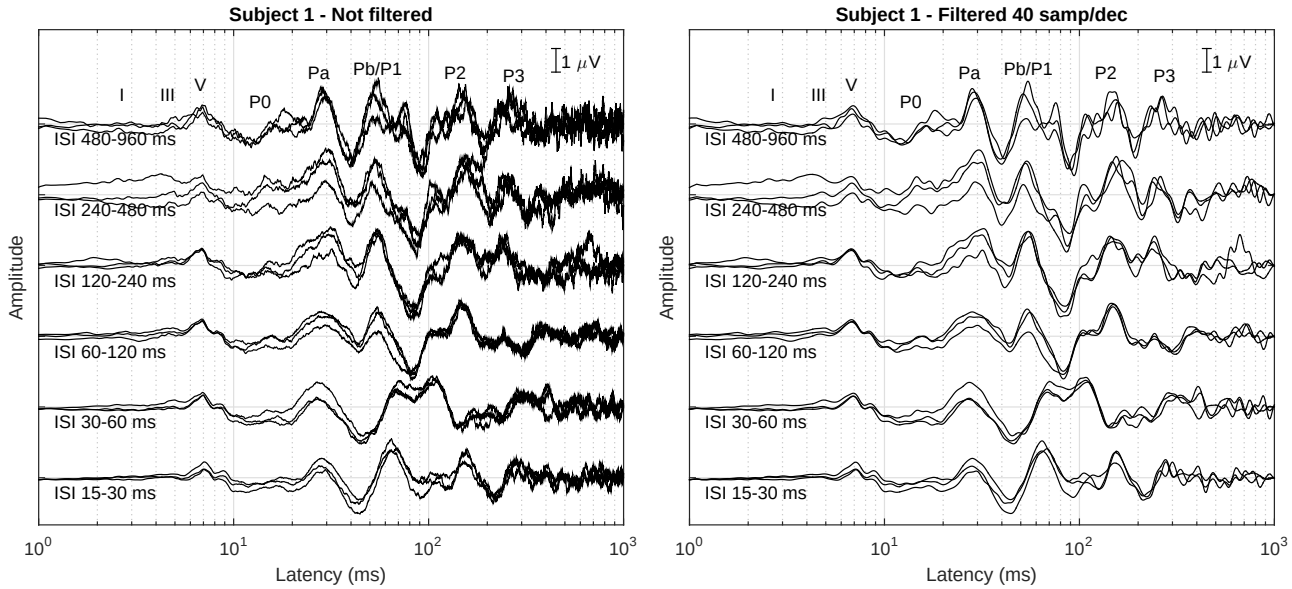

FIG. 5. AEP responses for Subject 1 without and with latency-dependent low-pass filtering (left and right panels, respectively).

AEP responses, while those in the right panel correspond to the latency-dependent filtered ones. At early latency, the plots without and with filtering are similar. However, at late latency, the not filtered responses are strongly affected by noise and the latency-dependent filtering provides an effective noise reduction with an evident quality improvement. Section 12.1 of the supplementary materials[1] includes similar plots for the eight subjects included in this study. The results in figure 5 are consistent with those in the simulations and also with those for the rest of subjects.

Figure 6 shows the SNR results with real AEP responses, for both the grand-average-based (averaged for the six stimulation conditions) and the subject-based (averaged for the six stimulation conditions and the eight subjects) estimations, as a function of the resolution. In the case of subject-based estimations, the SNR progressively increases as the resolution decreases, from 7.54 dB (not filtered responses) up to 10.74 dB (for resolution K_{dec}=15

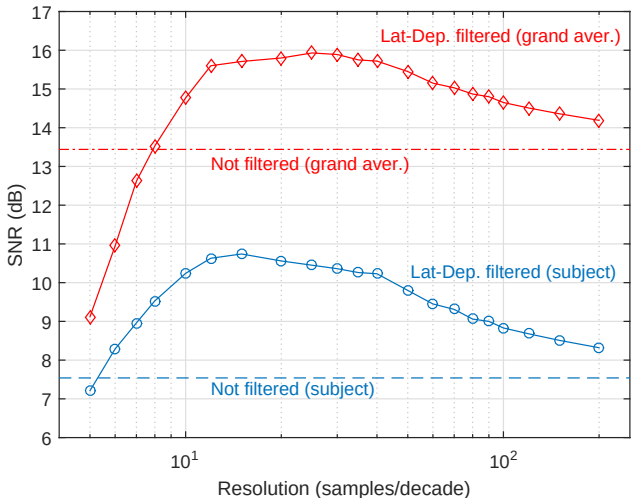

FIG. 6. (Color online) SNR of the real AEP responses as a function of the resolution K_{dec} used in the latency-dependent filtering, for both grand-average-based and subject-based estimations. The dashed lines represent the SNR for the not-filtered responses.

samples/decade) because the high-frequency noise is more effectively reduced by a more restrictive latency-dependent low-pass filtering. Below this resolution, the SNR decreases due to the distortion caused by the application of a too restrictive low-pass filtering. In the case of the grand-average-based estimations, the SNR is higher (for both the not-filtered and the latency-dependent filtered responses) and the maximum SNR (15.93 dB) is achieved at K_{dec}=25 samples/decade. Since the noise level is smaller in the grand-average responses, the highest SNR is achieved at a resolution slightly greater than in the previous case, and as expected, the best resolution depends on the noise level. According to this analysis, the most appropriate resolution depends on the noise level and would be in the range between 15 and 40 samples/decade, requiring 50 and 117 samples in the reduced representation, respectively. The supplementary materials[1] (Sections 12.2 and 12.3) include detailed results of the latency-dependent filtered AEP responses and SNRs at different resolutions.

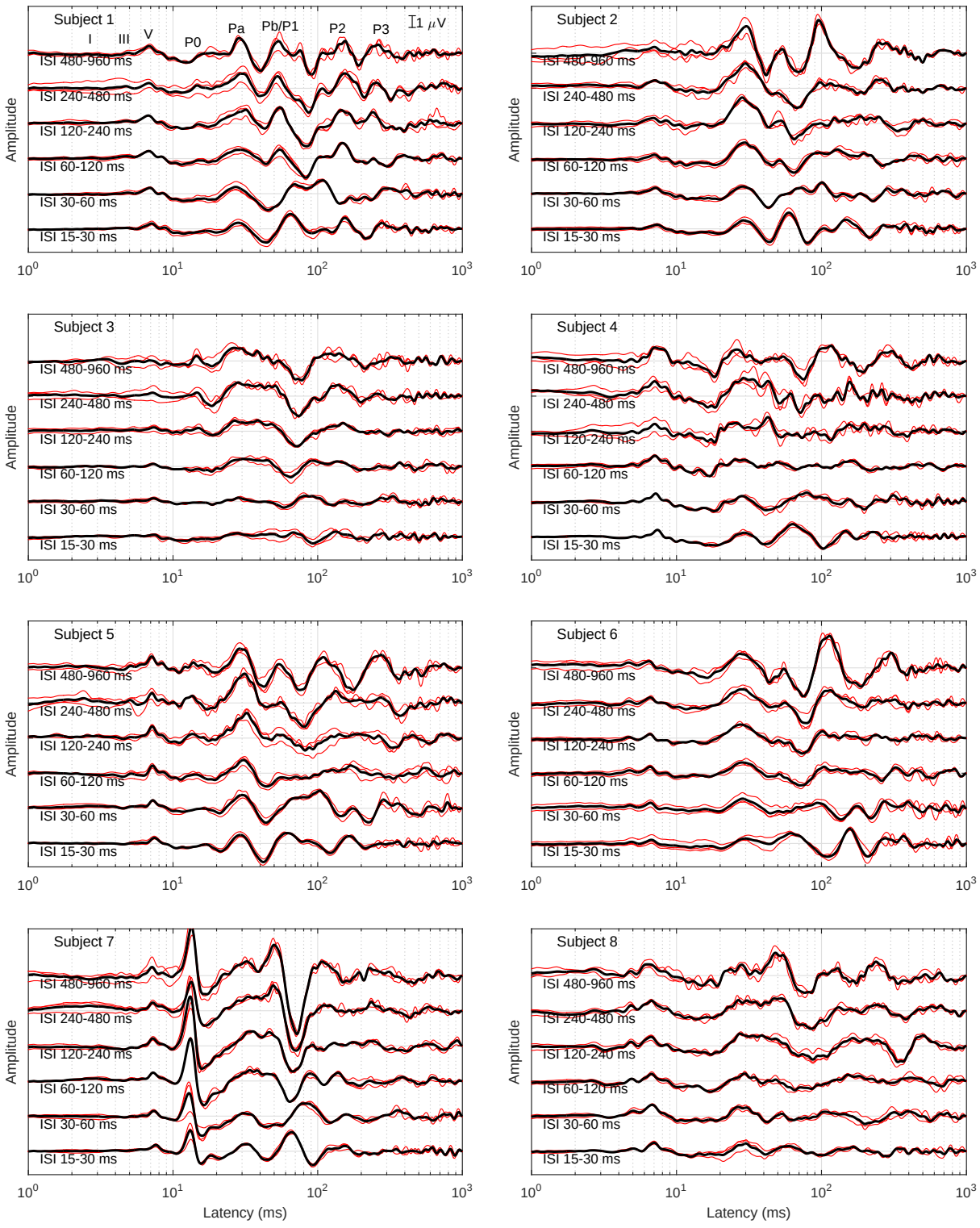

FIG. 7. (Color online) AEP responses estimated for all the subjects with latency-dependent filtering. Filtering configured with 40 samples/decade and responses reconstructed with 200 samples/decade between 1 and 1 000 ms. Thin lines are the individual AEP responses estimated from 228 s EEG portions; thick lines are the average AEP responses from the three EEG portions (684 s) for each subject and stimulation condition.

D. Representation of the complete auditory pathway response

The compact representation with 117 samples (for K_{dec}=40 samples/decade) for each AEP response is appropriate for data storage or for advanced data processing procedures (for instance classification or parameterization of responses (Valderrama *et al.*, 2014c)), since it minimizes the redundancy without relevant information loss. However, the compact representation $\mathbf{x}_r = V_r \cdot \mathbf{x}$ is not appropriate for a visual inspection by an audiologist or for comparison with conventional AEP responses, because the orthonormalization produces a latency-dependent alteration of the amplitude (as discussed in section II G). The reconstructed version (in the original representation) is easily obtained as $\mathbf{x}_{lp} = V_r^T \cdot \mathbf{x}_r$, but this representation is extremely redundant (14 700 samples required for each AEP response). In order to minimize this redundancy and at the same time provide a representation appropriate for an audiological analysis, we have reconstructed the responses with a resolution of 200 samples/decade in the interval 1-1 000 ms (i.e., three decades), therefore obtaining a representation requiring 600 samples.

Figure 7 represents the AEP responses, for the eight subjects included in this study, latency-dependent filtered with resolution of 40 samples/decade and reconstructed in the interval 1-1 000 ms with 200 samples/decade. For each stimulation condition, three responses are shown (estimated from each 228 s EEG portion) as well as the average (from the whole 684 s EEG) in order to allow the evaluation of the responses consistency. The most relevant waves are marked in the plot for subject 1. As observed in this figure, most of the AEP waves (including ABR, MLR and CAEP components) are consistently identified in all subjects.

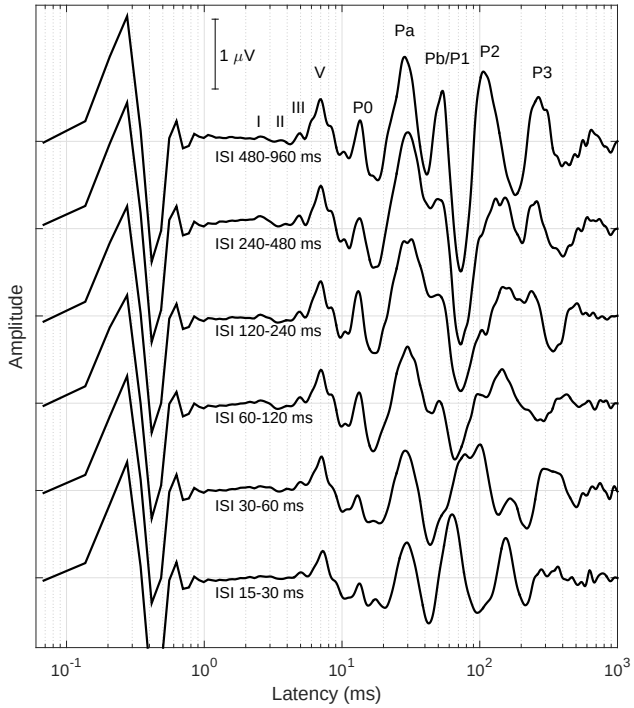

FIG. 8. Grand average of the AEP responses filtered with a resolution of 40 samples/decade reconstructed in the interval between 60 μs and 1 000 ms.

Additionally, some changes in the AEP response morphology associated to the stimulation rate are appreciated, particularly for the MLR and CAEP components. These changes are consistent across subjects, and reflect how both peripheral and central structures of the ascending auditory pathway respond to different acoustic scenarios. This figure also shows that the responses obtained from subject 7 are affected by the post-auricular muscle (PAM) artifact, a strong component of myogenic origin that appears at around 15 ms from stimulus onset (Pratt, 2007).

Figure 8 provides the grand-average of the AEP responses obtained from the eight subjects filtered with a resolution of 40 samples/decade and reconstructed in the interval between 60 μs and 1 000 ms (in order to provide, in addition to the evoked response, the

stimulus artifact and some pre-stimulus response). According to the synchronization configuration, the AEP waves in this figure (as in the rest of figures) are affected by a group delay of about 1 ms. The stimulation artifact in the interval 100-600 μs can be observed before the ABR waves. Since the different stimulation conditions only differs in the stimulation rate (but not in the stimulation level) the artifact is similar for all the conditions. This figure clearly shows changes in the morphology of the MLR and CAEP components associated to the stimulation rate. The supplementary materials[1] (Section 13) compares the grand-average responses with and without the latency-dependent filtering.

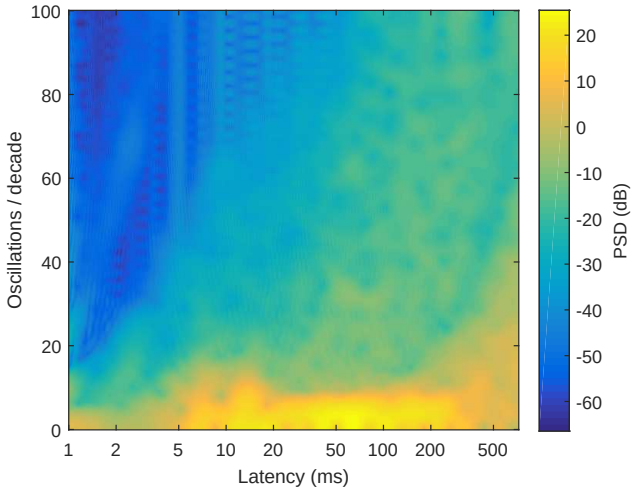

FIG. 9. (Color online) Average spectrogram of the log-scaled-latency AEP responses: power spectral density as a function of the number of oscillations per decade (vertical axis) and the log-scaled latency (horizontal axis).

E. Spectral distribution of the energy in the AEP responses

The expected morphology of the AEP responses suggests a limit for the number of oscillations per decade associated to the response waves. On the other hand, the latency-dependent

low-pass filtering and down-sampling with 40 samples/decade have provided consistent AEP responses. In order to investigate the spectral distribution of the energy in the AEP responses, we propose a spectral analysis with a logarithmic compression of the latency axis, which allows the estimation of the power spectral density (PSD) as a function of the number of oscillations per decade. We have estimated the spectrogram of the AEP responses filtered with K_{dec}=200 samples/decade and reconstructed with 200 samples/decade in the interval 0.6-1 000 ms. Figure 9 shows the spectrogram (resulting from averaging the spectrograms for the eight subjects and the six stimulation conditions). The colormap represents the PSD as a function of the latency (log-scaled, in the horizontal axis) and the number of oscillations per decade (in the vertical axis). In this diagram, the frequency can be estimated as $f(t, f_{dec}) = f_{dec}/(t \cdot \ln(10))$, where t is the latency and f_{dec} is the frequency expressed in oscillations per decade.

As observed in the average spectrogram, most of the energy is below 15 oscillations/decade (which is consistent with the spectral content expected in the evoked potentials at different latencies, (Burkard and Don, 2007; Martin *et al.*, 2007; Pratt, 2007)). This support the use of resolutions around 30 or 40 samples/decade in the latency-dependent low-pass filtering and down-sampling procedure. Additionally, this figure shows that AEP responses (which are not stationary processes since the spectral content strongly depends on the latency) can be considered a quasi-stationary process in the interval 2-300 ms when represented as a function of the compressed latency axis. This supports the latency-dependent filtering and down-sampling procedure proposed in this article. The energy above 10 oscillations/decade observed for latency greater than 300 ms correspond to brain waves (not synchronized with

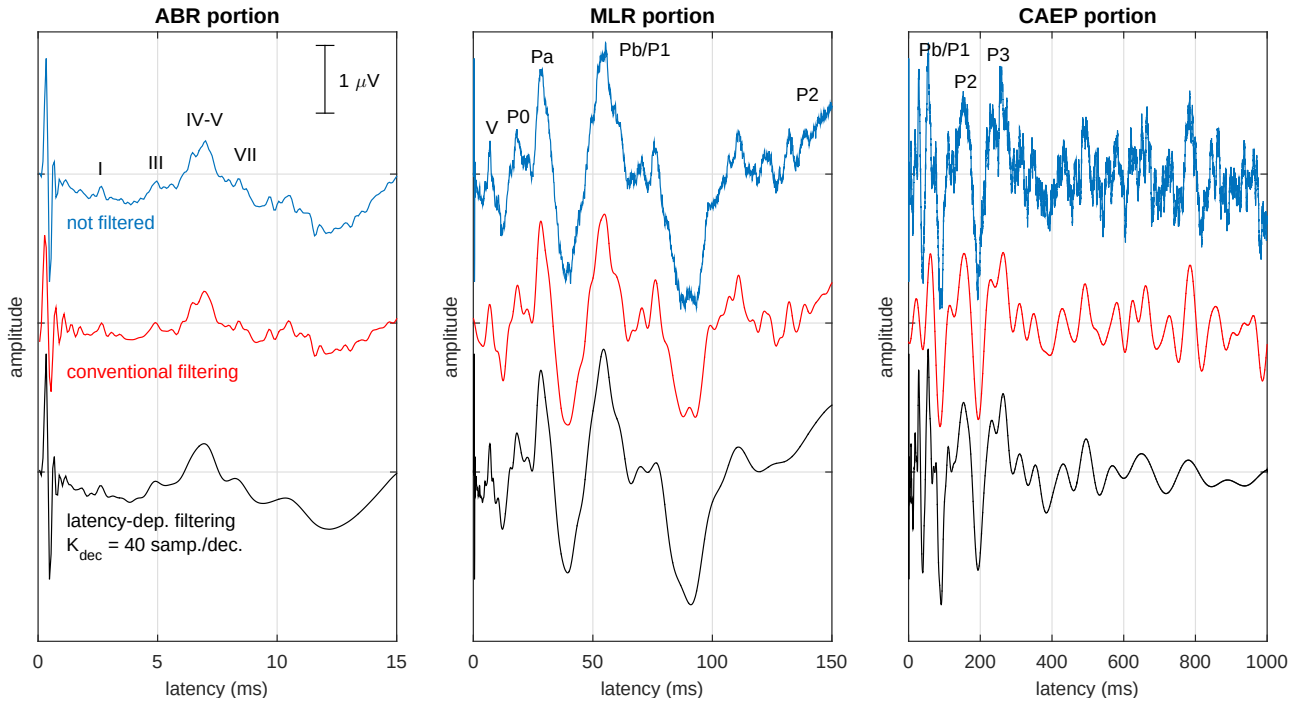

FIG. 10. (Color online) Conventional representation of the AEP responses for ABR, MLR and CAEP components. Responses from a 228 s EEG portion from subject 1, with stimulation configured for ISI=480-960 ms. In each figure, the not-filtered response (top) the response filtered with conventional filtering (middle) and the latency-dependent filtered response (bottom) are compared.

auditory stimulation, and therefore noise of neural origin for the AEP responses). Taking into account the frequency content of this noise, this activity probably corresponds to alpha or beta brain waves (the band 10-30 oscillations/decade at 500 ms latency corresponds to the band 8.6-26 Hz). The portion with the lowest energy (below 40 dB) at early latency and high frequency is associated to frequency components above 7 350 Hz (i.e., half of the original sampling rate). Section 14 of the supplementary materials[1] provides a more complete analysis of the spectral distribution of the AEP responses, including the average PSD as a function of the number of oscillations per decade.

F. Comparison with the conventional filtering of AEP components

The proposed latency dependent filtering was compared with conventional filtering applied to the ABR, MLR and CAEP portions of the AEP responses. In order to compare both, each portion was represented in the corresponding latency range, with a linearly scaled latency axis. In this comparison, the conventional filtering was implemented with band-pass zero-phase FIR filters with bandwidths 100-3000 Hz for the ABR portion, 10-300 Hz for the MLR portion and 1-30 Hz for the CAEP portion. The latency-dependent low-pass filtering was configured for a resolution K_{dec}=40 samples/decade. Figure 10 compares the conventional and the latency dependent filtering for the ABR, MLR and CAEP portions. The not-filtered responses are also included as reference. This response corresponds to the AEP estimation from a 228 s EEG portion recorded from subject 1 at ISI configuration 480-960 ms. Since the response was estimated from a relatively short EEG portion, it is strongly affected by noise, and the effect of the noise is better observed. Similar figures for a response estimated from a longer EEG (684 s) and grand average responses from the eight subjects (less affected by the noise) can be found in the supplementary materials[1] (Section 15).

As can be appreciated in this figure, both the conventional and the latency-dependent filtering provide an effective reduction of the high frequency noise, and a good synchronization of the waves (there is no latency distortion since both methods apply zero-phase filters). However, there are differences between the filtered responses provided by both methods. The conventional filtering is too restrictive at the early portion of the responses, and too permissive in the late portion. This produces a distortion of the ABR components in the MLR

plot, and of the MLR components in the CAEP plot, while noise is insufficiently attenuated at the late portions of the responses. The better preservation of the wave components and the more effective noise reduction provided by the latency-dependent filtering is associated to the continuous variation of the bandwidth with the latency. Additionally, the proposed method avoids the discontinuity imposed to the conventional AEP analysis, allowing a more comprehensive interpretation of the responses of the complete auditory pathway (as can be observed in figures 7 and 8).

There are also slight differences in the low frequency components of the responses filtered by both methods. Since the conventional filter applies band-pass filtering (but the proposed latency-dependent filtering is low-pass) some low frequency components are attenuated in the former but are not in the latter (this is evident, for example, in the last portion of the ABR response). High-pass filtering is particularly necessary when an isolated portion (for example ABR) is estimated with stimulation at high rate, in order to avoid the interference from late components elicited from the adjacent stimuli. However, in the experiments included in the present study, this interference is minimized since the whole AEP response (including ABR, MLR and CAEP components) is modeled and a deconvolution procedure (rather than a simple average) is applied for the response estimation, and the estimations provided by the latency-dependent low-pass filtering are appropriate. In any case, the proposed method could be easily adapted in order to provide band-pass filtering instead of low-pass filtering.

IV. DISCUSSION AND CONCLUSIONS

In this article we present a procedure providing latency-dependent low-pass filtering and down-sampling to be applied to AEP responses from the complete auditory pathway. The procedure is formulated as a matrix operation. An orthonormal matrix V_r applied to the original AEP response provides its projection in the subspace of the latency-dependent band-limited functions, i.e., a compact representation of the filtered signal. The compact representation can be transformed to the original representation (using the transposed V_r^T matrix) or, alternatively, the response can be reconstructed at a specific set of latencies.

The latency-dependent filtering and down-sampling is implemented by applying a uniform filtering and down-sampling in the compressed latency axis, using root-raised cosine sampling functions. A linear-logarithmic compression (with a resolution specified in terms of the number of samples per decade) has been applied.

The proposed procedure has been evaluated with both simulations and real AEP responses. In the experiments presented in this paper the dimensionality has been reduced from 14 700 samples (in the original representation) to 117 samples (in the compact representation for a resolution of 40 samples/decade). The procedure provides a significant quality improvement of the AEP responses, associated to the reduction of the high frequency noise at late latency. This improvement is clearly observed in the appearance of the responses and was objectively measured in terms of the SNR. For resolutions from 200 to 40 or 30 samples/decade, the dimensionality reduction is accompanied of quality improvement. Below 30

or 20 samples/decade (depending on the noise affecting the responses) the dimensionality can be reduced but the quality degrades due to the distortion of the waves.

The proposed method allows an adequate filtering and representation of the complete auditory pathway response. When the auditory response is estimated separately (i.e., when ABR, MLR or CAEP are independently measured), the conventional filtering and the uniform sampling are appropriate (because each portion is contained in just one decade of latency). However, conventional filtering and sampling are not appropriate for the response of the complete auditory pathway (covering almost three decades) because of the noise effect and the redundant representation. The alternative of representing each portion of the auditory response separately creates an artificial discontinuity between the waves in the different portions, not appropriate for global analysis and interpretation of the evoked responses. The latency-dependent filtering and down-sampling locally approaches the filtering and sampling-rate conventionally applied for ABR, MLR and CAEP, but at the same time eliminates the discontinuity between the different portions. This way, the proposed procedure offers new perspectives for the design of audiological experiments and for the analysis of evoked responses, allowing the simultaneous study of all the waves generated by the complete auditory pathway. While conventional filtering applies band-pass filtering, the proposed latency-dependent filtering applies a low-pass filtering. This is not a strong limitation for the representation of the complete auditory pathway, since the deconvolution applied to obtain the AEP responses avoids the interference of the late components over the early components. However the proposed latency-dependent filtering can be adapted for band-pass filtering, of potential utility for other audiological experiments. The proposed

filter design with zero-phase RRC filters guarantees that the latencies of the waves are not delayed by the procedure, but the non-causality associated zero-phase filters should be taken into consideration, depending on the purpose of the AEP analysis (de Cheveigne and Nelken, 2019).

This manuscript includes a study of the spectral content of the AEP responses. From the responses represented in the log-scaled latency axis, the AEP responses can be considered a quasi-stationary process, at least in the interval 2-300 ms. This quasi-stationarity of the responses has allowed the effective reduction of the noise without distortion by applying the latency-dependent filtering. The spectral analysis with the log-scaled latency axis also reveals that the spectral range below 7 oscillations/decade accumulates 95% of the AEP energy (see the supplementary materials [1], Section 14). This suggests that in the case of responses severely affected by noise, a more aggressive latency-dependent filtering (for instance with 20 or 15 samples/decade) would be useful (since in spite of the distortion of some waves, most of the shape of the AEP would be preserved).

In this article, the compression of the latency axis was performed with the relatively simple linear-logarithmic compression. More flexible compression functions could be applied in order to obtain a more accurate control of the local sampling frequency for each latency, or even for including pre-stimulus negative latency also with compression (i.e. including, with appropriate latency compression, portions where the response is expected to be null), in order to help the audiologist in the verification of the AEP response consistency, or in order to allow an evaluation of the SNR based on the pre-stimuli response (Polonenko and Maddox, 2019).

The advantages of the proposed procedure are obtained with a minimum computational cost, since only a matrix product is required. Additionally, the procedure provides a compact representation of the AEP responses (i.e., with the minimum number of samples and without information loss), which reduces the requirements for storage or transmission of AEP databases (of potential utility, for example, for remote AEP recording or monitoring). It can be also applied for reducing the computational cost of deconvolution algorithms for AEP responses (for example the IRSA algorithm could be equivalently applied in the original or in the reduced representation space, with a substantial reduction of the memory requirements and execution time in the reduced representation space). On the other hand, the concentration of the relevant information in a reduced number of samples simplifies the post-processing of AEP data. Algorithms for classification, characterization or parameterization of waves or AEP responses (Bradley and Wilson, 2005; Fridman *et al.*, 1982; Kamerer *et al.*, 2020; Valderrama *et al.*, 2014c), as well as procedures based on artificial intelligence, involving deep artificial neural networks or designed under the perspective of big-data analysis (Dobrowolski *et al.*, 2016; Mosqueda-Cárdenas *et al.*, 2019) would benefit from compacting the relevant information in low-dimensionality vectors (Trunk, 1979).

The procedures for latency-dependent low-pass filtering and down-sampling and for the response reconstruction have been implemented as MatLab/Octave functions and are provided in the supplementary materials[1] (Sections 6 and 9, respectively). A MatLab/Octave script has also been prepared for running a demonstration involving the proposed procedures (see the supplementary material[1], Section 16). The script reads an AEP response, estimates the latency-dependent filtering and down-sampling matrix and the reconstruction

matrix for the specified resolutions, and represents the not filtered responses as well as the filtered responses (a) in the reduced representation, (b) in the original representation, and (c) at the latencies specified for reconstruction. The script also plots the functions of the basis. Additionally, in order to provide the community with these computational tools, MatLab/Octave functions and scripts as well as data with examples have been included in a compressed directory in the supplementary materials[1].

ACKNOWLEDGMENTS

This work was partially supported by the Spanish Ministry of Science, Innovation and Universities under the project EQC2018-004988-P. The authors acknowledge the constructive revision of the anonymous reviewers.

[1]See the supplementary materials at [URL will be inserted by AIP] for a PDF file presenting (section 1) a description of the matrix implementation of low-pass filtering and down-sampling; (section 2) a description of the matrix implementation of the latency-dependent low-pass filtering and down-sampling; (section 3) the derivation of the linear-logarithmic compression of the latency axis; (section 4) a description of the root-raised cosine filters; (section 5) a description of the latency-dependent filtering and down-sampling using RRC filters; (section 6) MatLab/Octave code providing the latency-dependent filtering and down-sampling matrix; (section 7) a description of the functions in the orthonormal basis; (section 8) a description of the procedure for response reconstruction at a specified set of latencies; (section 9) MatLab/Octave code providing the reconstruction matrix; (section 10) a description of the response used for the simulations; (section 11) detailed experimental results with simulations; (section 12) detailed experimental results with real responses; (section 13) grand average of the responses of the auditory pathway; (section 14) spectral analysis of the AEP responses; (section 15) MatLab/Octave code of a script for testing the latency-dependent filtering and down-sampling. A compressed directory with examples and MatLab/Octave scripts and functions, aiming to help the reader apply the latency-dependent low-pass filtering and down-sampling procedure described in this paper is also included in the supplementary materials.

Bardy, F., Dillon, H., and Dun, B. V. (**2014**a). "Least-squares deconvolution of evoked potentials and sequence optimization for multiple stimuli under low-jitter conditions," Clinical Neurophysiology **125**, 727–737.

Bardy, F., Dun, B. V., Dillon, H., and McMahon, C. M. (**2014**b). "Deconvolution of overlapping cortical auditory evoked potentials recorded using short stimulus onset-asynchrony ranges," Clinical Neurophysiology **125**, 814–826.

Bohorquez, J., and Ozdamar, O. (**2006**). "Signal to noise ratio analysis of maximum length sequence deconvolution of overlapping evoked potentials," Journal of the Acoustical Society of America **119**, 2881–2888.

Bradley, A. P., and Wilson, W. J. (**2005**). "Automated analysis of the auditory brainstem response using derivative estimation wavelets," Audiology and Neuro-Otology **10**, 6–21.

Burkard, R. F., and Don, M. (**2007**). "The auditory brainstem response," in *Auditory evoked potentials: basic principles and clinical application*, edited by R. Burkard, M. Don, and J. Eggermont (Lippincott Williams & Wilkins, Baltimore), pp. 229–253.

de Cheveigne, A., and Nelken, I. (**2019**). "Filters: When, why, and how (not) to use them," Neuron **102**, 280–293.

de la Torre, A., Valderrama, J. T., Segura, J. C., and Alvarez, I. M. (**2019**). "Matrix-based formulation of the iterative randomized stimulation and averaging method for recording evoked potentials," Journal of the Acoustical Society of America **146**, 4545–4556.

Dobrowolski, A., Suchocki, M., Tomczykiewicz, K., and Majda-Zdancewicz, E. (**2016**). "Classification of auditory brainstem response using wavelet decomposition and svm network," Biocybernetics and Biomedical Engineering **36**, 427–436.

718 Elberling, C., Kristensen, S. G. B., and Don, M. (**2012**). "Auditory brainstem responses
719 to chirps delivered by different insert earphones," Journal of the Acoustical Society of
720 America **131**, 2091–2100.
721 Eysholdt, U., and Schreiner, C. (**1982**). "Maximum length sequences: A fast method for
722 measuring brain-stem-evoked responses," Audiology **21**, 242–250.
723 Fridman, J., John, E. R., Bergelson, M., Kaiser, J. B., and Baird, H. W. (**1982**). "Ap-
724 plication of digital filtering and automatic peak detection to brain stem auditory evoked
725 potential," Electroencephalography and Clinical Neurophysiology **53**, 405–416.
726 Gillespie, P. G., and Muller, U. (**2009**). "Mechanotransduction by hair cells: Models,
727 molecules, and mechanisms," Cell **139**, 33–44.
728 Holt, F., and Ozdamar, O. (**2016**). "Effects of rate (0.3-40/s) on simultaneously recorded
729 auditory brainstem, middle and late responses using deconvolution," Clinical Neurophysi-
730 ology **127**, 1589–1602.
731 Jewett, D. L., Caplovitz, G., Baird, B., Trumpis, M., Olson, M. P., and Larson-Prior,
732 L. J. (**2004**). "The use of qsd (q-sequence deconvolution) to recover superposed, transient
733 evoked-responses," Clinical Neurophysiology **115**, 2754–2775.
734 Kamerer, A. M., Neely, S. T., and Rasetshwane, D. M. (**2020**). "A model of auditory
735 brainstem response wave i morphology," Journal of the Acoustical Society of America
736 **147**, 25–31.
737 Kohl, M. C., Schebsdat, E., Schneider, E. N., Niehl, A., Strauss, D. J., Ozdamar, O.,
738 and Bohorquez, J. (**2019**). "Fast acquisition of full-range auditory event-related potentials
739 using an interleaved deconvolution approach," Journal of the Acoustical Society of America

145, 540–550.

Lütkenhöner, B. (**2010**). "Baseline correction of overlapping event-related responses using a linear deconvolution technique," NeuroImage **52**, 86–96.

Maddox, R. K., and Lee, A. K. C. (**2018**). "Auditory brainstem responses to continuous natural speech in human listeners," eNeuro **5**, e0441, 13p.

Martin, B. A., Tremblay, K. L., and Stapells, D. R. (**2007**). "Principles and applications of cortical auditory evoked potentials," in *Auditory evoked potentials: basic principles and clinical application*, edited by R. Burkard, M. Don, and J. Eggermont (Lippincott Williams & Wilkins, Baltimore), pp. 482–507.

Mosqueda-Cárdenas, E., de la Rosa-Gutiérrez, J. P., Aguilar-Lobo, L. M., and Ochoa-Ruiz, G. (**2019**). "Lecture notes in computer science (including subseries lecture notes in artificial intelligence and lecture notes in bioinformatics)," in *11th Mexican Conference on Pattern Recognition, MCPR 2019*, Querétaro; Mexico, pp. Volume 11524 LNCS, 2019, Pages 227–237.

Ozdamar, O., and Bohorquez, J. (**2006**). "Signal-to-noise ratio and frequency analysis of continuous loop averaging deconvolution (clad) of overlapping evoked potentials," Journal of the Acoustical Society of America **119**, 429–438.

Polonenko, M. J., and Maddox, R. K. (**2019**). "The parallel auditory brainstem response," Trends in Hearing **23**, 1–17.

Pratt, H. (**2007**). "Middle-latency responses," in *Auditory evoked potentials: basic principles and clinical application*, edited by R. Burkard, M. Don, and J. Eggermont (Lippincott Williams & Wilkins, Baltimore), pp. 463–481.

762 Proakis, J. G., and Salehi, M. (**2008**). *Digital Communications*, 1150 p., 5^{th} ed. (McGraw-
763 Hill, New York).
764 Thornton, A. R. D. (**2007**). "Instrumentation and recording parameters," in *Auditory evoked*
765 *potentials: basic principles and clinical application*, edited by R. Burkard, M. Don, and
766 J. Eggermont (Lippincott Williams & Wilkins, Baltimore), pp. 73–101.
767 Thornton, A. R. D., and Coleman, A. (**1975**). "The adaptation of cochlear and brainstem
768 auditory evoked potentials in humans," Electroencephalograpy and Clinical Neurophysiol-
769 ogy **39**, 399–406.
770 Thornton, A. R. D., and Slaven, A. (**1993**). "Auditory brainstem responses recorded at
771 fast stimulation rates using maximum length sequences," British Journal of Audiology **27**,
772 205–210.
773 Trunk, G. V. (**1979**). "A problem of dimensionality: a simple example," IEEE Transactions
774 on Patterns Analysis and Machine Intelligence **1**, 306–307.
775 Valderrama, J. T., Alvarez, I., de la Torre, A., Segura, J. C., Sainz, M., and Vargas, J. L.
776 (**2012**). "Recording of auditory brainstem response at high stimulation rates using ran-
777 domized stimulation and averaging," Journal of the Acoustical Society of America **132**,
778 3856–3865.
779 Valderrama, J. T., de la Torre, A., Alvarez, I., Segura, J. C., Sainz, M., and Vargas, J. L.
780 (**2013**). "A portable, modular, and low cost auditory brainstem response recording sys-
781 tem including an algorithm for automatic identification of responses suitable for hearing
782 screening," in *Proceedings of the IEEE/EMBS Special Topic Conference on Point-of-Care*
783 *HealthCare Technologies (PoCHT)*, Bangalore, India, pp. 180–189 (art. no. 6461314).

Valderrama, J. T., de la Torre, A., Alvarez, I., Segura, J. C., Sainz, M., and Vargas, J. L. (**2014**a). "A flexible and inexpensive high-performance auditory evoked response recording system appropriate for research purposes," Biomedical Engineering / Biomedizinische Technik **59**, 447–459.

Valderrama, J. T., de la Torre, A., Alvarez, I., Segura, J. C., Thornton, A. R. D., Sainz, M., and Vargas, J. L. (**2014**b). "Auditory brainstem and middle latency responses recorded at fast rates with randomized stimulation," Journal of the Acoustical Society of America **136**, 3233–3248.

Valderrama, J. T., de la Torre, A., Alvarez, I., Segura, J. C., Thornton, A. R. D., Sainz, M., and Vargas, J. L. (**2014**c). "Automatic quality assessment and peak identification of auditory brainstem responses with fitted parametric peaks," Computer Methods and Programs in Biomedicine **114**, 262–275.

Valderrama, J. T., de la Torre, A., and Dun, B. V. (**2018**). "An automatic algorithm for blink-artifact suppression based on iterative template matching: Application to single cannel recording of cortical auditory evoked potentials," Journal of Neural Engineering **15**(016008), 016008, 15p.

Valderrama, J. T., de la Torre, A., Medina, C., Segura, J. C., and Thornton, A. R. D. (**2016**). "Selective processing of auditory evoked responses with iterative-randomized stimulation and averaging: A strategy for evaluating the time-invariant assumption," Hearing Research **333**, 66–76.

Woldorff, M. G. (**1993**). "Distortion of erp averages due to overlap from temporally adjacent erps: Analysis and correction," Psychophysiology **30**, 98–119.